ACS Chemical Neuroscience

Research Article

pubs.acs.org/chemneuro

Antipsychotic Haloperidol Binding to the Human Dopamine D3 Receptor: Beyond Docking Through QM/MM Refinement Toward the Design of Improved Schizophrenia Medicines

Geancarlo Zanatta,*[,†] Gustavo Nunes,[†] Eveline M. Bezerra,[‡] Roner F. da Costa,[§] Alice Martins,[‡] Ewerton W. S. Caetano,[∥] Valder N. Freire,[⊥] and Carmem Gottfried[†]

[†]Department of Biochemistry, Federal University of Rio Grande do Sul, 90035-003 Porto Alegre, RS Brazil

[‡]Post-graduate Program in Pharmaceutical Sciences, Pharmacy Faculty, Federal University of Ceará, 60430-372 Fortaleza, CE Brazil

[§]Department of Physics, Universidade Federal Rural do Semi-Árido, 59780-000 Caraúbas, RN Brazil

[∥]Federal Institute of Education, Science and Technology, 60040-531 Fortaleza, CE Brazil

[⊥]Department of Physics, Federal University of Ceará, 60455-760 Fortaleza, CE Brazil

Supporting Information

ABSTRACT: As the dopamine D3R receptor is a promising target for schizophrenia treatment, an improved understanding of the binding of existing antipsychotics to this receptor is crucial for the development of new potent and more selective therapeutic agents. In this work, we have used X-ray cocrystallization data of the antagonist eticlopride bound to D3R as a template to predict, through docking essays, the placement of the typical antipsychotic drug haloperidol at the D3R receptor binding site. Afterward, classical and quantum mechanics/molecular mechanics (QM/MM) computations were employed to improve the quality of the docking calculations, with the QM part of the simulations being accomplished by using the density functional theory (DFT) formalism. After docking, the calculated QM improved total interaction energy E_{QMDI} = −170.1 kcal/mol was larger (in absolute value) than that obtained with classical molecular mechanics improved (E_{CLDI} = −156.3 kcal/mol) and crude docking (E_{CRDI} = −137.6 kcal/mol) procedures. The QM/MM computations reveal the pivotal role of the Asp110 amino acid residue in the D3R haloperidol binding, followed by Tyr365, Phe345, Ile183, Phe346, Tyr373, and Cys114. Besides, it highlights the relevance of the haloperidol hydroxyl group axial orientation, which interacts with the Tyr365 and Thr369 residues, enhancing its binding to dopamine receptors. Finally, our computations indicate that functional substitutions in the 4-clorophenyl and in the 4-hydroxypiperidin-1-yl fragments (such as C3H and C12H hydrogen replacement by OH or COOH) can lead to haloperidol derivatives with distinct dopamine antagonism profiles. The results of our work are a first step using in silico quantum biochemical design as means to impact the discovery of new medicines to treat schizophrenia.

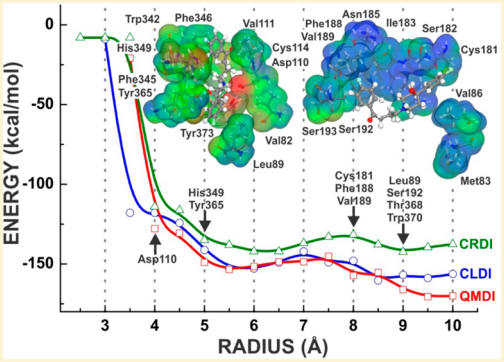

KEYWORDS: *Quantum biochemistry, dopamine receptor, haloperidol, D3 binding pocket, quantum mechanics, DFT, antipsychotic, ab initio, docking, QM/MM ONIOM method*

Schizophrenia is a mental illness affecting about five per thousand in population, varying across cultures and countries, and being more prevalent among males.[1] Symptoms are classified as positive (e.g., hallucination, delusions, etc.), negative (e.g., lack of pleasure, difficulties to begin and sustain activities, etc.) and cognitive (e.g., problems with executive functions, working memory, etc.).[2,3] Schizophrenia is a severe and disabling neurological disorder that typically begins in late adolescence or early adulthood, having a large impact on the patients and society. World Health Organization estimates of schizophrenia-related economic costs in 2001, available only for some industrialized countries, range between 1.6% and 2.6% of the total health care expenditures.[4] For England, it was estimated a £6.7 billion schizophrenia-related societal cost in 2004−2005.[5] In the United States, the cost of schizophrenia was estimated to be $62.7 billion in 2002.[6]

Antipsychotics began to be introduced for the treatment of schizophrenia in the 1950s. Many of them exert their therapeutic effects through the blockage of the dopamine receptors group.[7−9] Binding profile, type of side effect events, and mechanisms of action, among other characteristics, are used to characterize antipsychotics as first- and second-generation agents (also known as typical and atypical, respectively).[7,8,10] Typical antipsychotics (e.g., chlorpromazine,

Received: May 16, 2014
Revised: September 1, 2014
Published: September 2, 2014

ACS Publications © 2014 American Chemical Society

fluphenazine, and haloperidol) are known to block the D2R dopamine receptor (see below) in the mesolimbic and nigrostriatal pathway, leading to extrapyramidal symptoms (EPS) and late dyskinesia. Atypical antipsychotics (e.g., clozapine, olanzapine, and risperidone) were introduced in the last three decades, being believed to be more efficacious, tolerable and associated with fewer EPS.[11]

A complete understanding of dopaminergic neurotransmission is highly important to enhance the treatment of schizophrenic conditions. Dopamine regulates its pathway through the coordinated activation of dopamine receptors: D1-like (D1R and D5R) and D2-like (D2R, D3R and D4R).[12,13] These receptors are G-protein-coupled (GPCR) (see the Nobel Prize in Chemistry lecture, 2012)[14−16] characterized by the presence of seven highly conserved transmembrane helices (TMH1-THM7), connected by extracellular (EC) and intracellular (IC) loops.[17,18] Receptors belonging to the D1-like family activate adenylyl cyclase through the stimulatory G-protein alpha subunit, while receptors of the D2-like family are coupled to the G-protein alpha subunit, with inhibitory effects over adenylyl cyclase.[19]

Among the dopamine receptors, the D3R subtype has been discovered as an important target for the treatment of schizophrenia, Parkinson's disease, and other neurological diseases.[20−22] In medicated schizophrenic patients, the D3R level was similar to or less than that in control levels, but is doubled in antipsychotics-free patients, suggesting that D3R is related to the antipsychotic efficacy in the treatment, while the D2R blockade is involved with exptrapyramidal side effects.[23] Analysis of post-mortem tissues showed D2R distribution in the dorsal putamen and the dorsal caudate nucleus, but not D3R. In the ventral putamem, ventral caudate, and globus pallidus, a D2R/D3R distribution in a 2:1 proportion was observed.[24] High D2R concentration in the striatum seems to be a target for antipsychotics and is related to motor side effects associated with the nigrostriatal region. In the mesolimbic region, D3R has an important role in the dopamine system[25] and its RNA encoding is abundant in the ventral area. Indeed, the understanding of the anatomical distribution of dopamine receptor subtypes in the central nervous system (CNS) is crucial to the rational development of subtype-selective agents in order to improve treatment efficacy, as well as to reduce side effects.[26−31] In this regard, it has been recognized that antagonism in D3R may represent a novel and potent antipsychotic mechanism devoid of EPS, making D3R a good target for the improved drug treatment of schizophrenia.[25,29]

Haloperidol, 4-[4-(4-chlorophenyl)-4-hydroxypiperidin-1-yl]-1-(4-fluorophenyl)butan-1-one, chemical formula $C_{21}H_{23}ClFNO_2$ (see Figure 1A), is a phenyl-piperidinyl-butirophenone. It was synthesized in 1958 by Janssen Pharmaceutical and can be considered a typical antipsychotic,[32] being an effective clinic agent employed in the therapy of the positive symptoms of schizophrenia, mania and neurological disorders.[33] It is argued that haloperidol acts through the blockade of dopamine D2-like receptors in the mesocortex and limbic systems of the brain.[34,35] Additionally, according to Malmberg and colleagues,[36] haloperidol is a D2R antagonist which also acts like an inverse agonist in D3R. Moreover, haloperidol also has an ability of binding to a wide variety of central nervous system receptors, such as the adrenergic and muscarinic ones, among others.[37]

The high homology degree of dopamine receptors explains the low specificity of haloperidol and other similar drugs. In

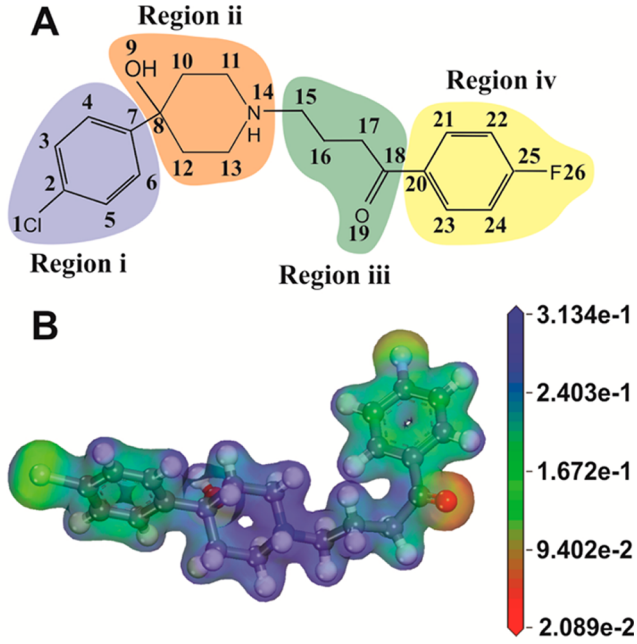

Figure 1. (A) Atom labels for haloperidol at physiological pH. Region i has the 4-clorophenyl fragment; region ii has the 4-hydroxypiperidin-1-yl fragment with the tertiary amine protonated; region iii has the butan-1-one fragment; and region iv has the 4-fluorophenyl fragment. (B) Electron density calculated using DFT projected onto an electrostatic potential isosurface. Negatively charged regions are in red, and positively charged regions are in blue, as depicted in the charge scale.

fact, it was highlighted that D2R and D3R share 46% homology, with 78% being in the transmembrane helices (TM).[25,38] Chien and colleagues[38] showed that, among 18 eticlopride contact residues in the binding pocket of D3R, 17 are identical to D2R residues, suggesting that such similarities in the binding pocket give rise to closely related affinities, as observed for many compounds. Although promoting the D2R dopamine blockade in the nigrostriatal region, triggering extrapyramidal symptoms (dyistonias, akathisia, late dyskinesia, and pseudoparkinsonism),[39] haloperidol is still widely used in clinic as the newer atypical antipsychotics have high cost, also being related to the development of important side effects, unhappily.[40−42]

In this work, due to the haloperidol clinical relevance and its ability to antagonize D3R, it was investigated its mode of interaction with individual residues of its D3R binding pocket. The results of this in silico research work are quite useful as a guide to the design of haloperidol derivatives with stronger D3R antagonism. The published crystallographic data of D3R complexed with eticlopride[38] was taken into account to simulate the docking of haloperidol in D3R by ligand replacement. Quantum mechanics/molecular mechanics (QM/MM) computation procedures were carried out to optimize molecular geometries within the density functional theory (DFT) formalism. The haloperidol−D3R amino acid residue interactions were evaluated using the divide-to-conquer-like molecular fractionation with conjugate caps (MFCC) technique.[43] A binding pocket radius r was defined, varying from 2.5 to 10.0 Å, being supposed to contain the most important D3R residues interacting with haloperidol. The interaction energies of haloperidol with individual amino acid

residues were estimated, providing a description of the dependence of the total binding energy with the binding pocket radius. Besides, functional substitutions in the 4-chlorophenyl and in the 4-hydroxypiperidin-1-yl fragments (such as C3H and C12H hydrogen replacement by OH, OOH, or Cl groups) were discovered as routes to search for haloperidol derivatives with distinct dopamine antagonism profiles. Our results are a first step toward in silico quantum biochemical design and probing of new medicines to treat schizophrenia.

RESULTS AND DISCUSSION

In the dopaminergic neuroscience domain, it is remarkable the recent publication of the D3R structure cocrystallized with eticlopride.[38] This work has motivated structure-based drug research through in silico simulations of ligands interaction with D3R. As a matter of fact, Feng and colleagues[44] have used molecular dynamics to refine docking results of selective ligands, highlighting the importance of Thr369 to the selectivity of R-22 with D3R. On the other hand, the D3R crystallographic structure was used to generate D2R and D3R models which were validated through the docking of distinct ligands, followed by molecular dynamics procedures.[45]

Docking algorithms have become popular in the field of computer-aided drug design because they are useful tools to predict the binding of small molecules to a protein structure.[46−48] However, due to the low accuracy of the score functions, it is often hard to find the best pose among docking results. To deal with this problem, more robust approaches can be employed. In this sense, QM methods,[49] which have been proving themselves to be of great importance in all phases of in silico drug design,[50] are becoming more popular due to their high accuracy to estimate (relative) binding affinities.[51] Nevertheless, the computational cost to simulate large systems at the QM level is very high because of the huge number of electrons involved. To overcome this difficulty, it is possible to describe the system by using its electron density $\rho(r)$, which depends on three spatial coordinates only, instead of the full electronic wave function, with $3N$ spatial coordinates (N being the total number of electrons involved). This is the essential feature of DFT, where the total energy of a multielectronic system is expressed as a functional of the electron density, leading to the so-called Kohn−Sham equations.[52,53] Besides, the divide-to-conquer-like MFCC scheme is most helpful to reduce the computational cost and preserving, at the same time, an accurate description of biological systems through quantum calculations.[43,54−57] In particular, our group has employed previously the MFCC method to describe ligand−protein interactions at the quantum level in other relevant biological systems.[58−62]

Another important issue related to ligand−protein docking is how to take into account the flexibility of the protein structure to make the results more realistic.[48,63] Among recent suggested strategies, one find the use of hybrid QM/MM approaches to carry out docking refinement.[49,64] The use of a hybrid method can be a good route for the study of large proteins, as it allows the partition of the entire system into two regions: (1) a small region of interest, which is described using QM methods, and (2) the rest of the protein system, which is modeled using a classical MM force field. Among the QM/MM methods, Own N-layer Integrated molecular Orbital molecular Mechanics (ONIOM) has been used with success to treat biological systems due to its simplicity and high accuracy.[65] By combining docking and ONIOM techniques, it is possible to achieve a reliable structure to investigate protein−ligand interactions at the molecular level through quantum biochemistry ab initio simulations; see the Nobel Prize in Chemistry lecture of 2013.[66]

In the work here presented, the X-ray data of eticlopride cocrystallized with the dopamine receptor D3 at 3.15 Å of resolution, PDB ID 3PBL,[38] was adopted as a template for the docking essays, with the purpose of replacing the etilclopride molecule by haloperidol. As a matter of fact, the docking of haloperidol in the rigid structure of the crystallographic D3R was performed in the original eticlopride binding site, which was followed by classical and QM/MM optimizations. Such geometry optimizations allowed some degree of flexibility in the binding pocket site of the receptor, which is fundamental for its function and drug design,[67] but is absent in the crude docking procedure.[47,68,69] Afterward, ligand−residue interaction energies were calculated using DFT through the MFCC scheme. The QM calculations were performed both in the local-density approximation (LDA)[70,71] and generalized gradient approximation approach with an extra dispersion correction scheme as proposed by Tkatchenko and Scheffler (GGA+TS).[72,73] These procedures enabled a better description of the haloperidol in its human D3R receptor binding pocket.

Haloperidol and Receptor Preparation. The protonation state of the ligand used in this study is in agreement with in vitro experiments which demonstrated that, among the use of charged and uncharged analogues of dopamine, the agonist activity is optimal for charged species.[74] Also, Chien and Colleagues[38] stated that the protonated ethyl-pyrrolidine ring of eticlopride, at physiological pH, is fundamental for the formation of a salt bridge with the carboxylate of Asp110, which is structural and pharmacologically critical for high affinity ligand binding to the aminergic subfamily of GPCRs. Such reports give us support to follow experiments using a protonation scheme reflecting the physiological pH, but considering variation due to the local protein environment. Calculations of haloperidol showed that in the 7.2−7.4 pH range there is a prevalence (97.34−95.85%) of protonation at the piperidine ring. Also, the protonation state of amino acid residues, at the physiological pH, was adjusted according to PROPKA tool results and the protonation tool in the Discovery Studio package (see Methods for more details). In this way, important residues within the radius of 10 Å from the centroid of haloperidol had their protonation adjusted according to results, such as Asp110 (pka 3.9) and His349 (pka 6.0), among others. Also, in order to improve the docking input, the protonated haloperidol molecule geometry was optimized through classical and quantum energy minimization steps, following the same protocol used to prepare the eticlopride for redocking. The haloperidol protonation considered during the docking runs is depicted in Figure 1, together with the electron density distribution of the isolated haloperidol molecular structure after DFT geometry optimization.

Docking Results and Selected Pose. Initially, the docking parameters were set through the application of a redocking protocol to the eticlopride−D3R system using Autodock 4.0. Two essays of redocking were performed, the simple one using the eticlopride structure as given by the crystallographic data, and an improved one where it was considered a quantum optimized built molecule (see Figure S1 in the Supporting Information). As no significant differences were observed between the redocking essays, the initial

structure of haloperidol was built and optimized using the same approach applied to generate the molecule of eticlopride through the redocking (see Methods) before being used for the docking in the rigid pocket of D3R. The tuning of the docking machinery for haloperidol was performed following the same steps of the eticlopride−D3R redocking. Docking experiments generated 1000 poses, which were clustered using a RMSD tolerance of 1.0 Å^2; the first pose of each cluster scored better than the threshold of −10 kcal/mol, being evaluated in a rescore procedure (see pose selection in Methods). This approach allowed us to quickly evaluate the docking score of 13 poses in order to choose the most representative of them. Probably because our calculation took into consideration all hydrogen atoms in the system (differently from the Autodock approach, which computes only the polar hydrogen atoms in the protein), which makes the calculation more accurate by allowing a more realistic spatial arrangement of the atoms during geometry optimizations, it was obtained a slightly different ranking of poses (see Table S1). Nevertheless, our rescore calculation confirmed as the best representative pose the same one indicated by the Autodock score (the first pose from the cluster 1). From now on, such pose will be labeled DOC. Moreover, during visual inspection it was observed that DOC represents the haloperidol orientation with the fluorine atom pointing toward Helix V, and the chlorine atom pointing toward Helix II, agreeing with the haloperidol orientation in D2R as indicated by Hjerde and colleagues.[75] However, it curiously differ from that obtained by Wang and colleagues,[76] which have obtained that the *para*-fluorophenyl plane is oriented along the Helix II in their modeling of D2 and D3 receptors. Also, it was observed that in DOC the haloperidol piperidine ring assumes a chair conformation, as described in the literature,[77,78] and also that the phenyl ring was oriented in the equatorial position while the hydroxyl group was oriented axially.[78]

Some of the discrepancies observed in published docking simulations can be due to methodological differences. As a matter of fact, Wang et al.[76] have used modeled structures in their study (the crystallographic data of D3R had not yet been published then), building the ligand haloperidol in situ and carrying out energy minimization steps followed by molecular dynamics (MD) calculations to refine the structures. As advanced by Sousa et al.,[47] MD is known to have several pitfalls when used in attempts to replace docking algorithms in ligand−protein systems, mainly due to difficulties in scanning over the typically rugged energy hypersurface of biological systems and in crossing high-energy barriers. Moreover, the simulation time could not be large enough to adequately sample the conformational space in such a way that a stabilized binding is not achieved.

Docking Refinement Through QM/MM Calculations. Considering that the side chains of proteins are supposed to reorganize in a wide range of ways within the binding pocket (backbone displacement is more rare),[79] we performed three distinct geometry optimization procedures for the sake of comparison and to improve the quality of the results. In the first procedure, hydrogen atoms were added to the DOC structure and only their positions were classically optimized to minimize the haloperidol−D3R total energy. From now on, this new geometry will be referred as crude docking input (CRDI) structure. In the second procedure, it was generated the classical mechanics docking input (CLDI) structure through the optimization of all hydrogen atoms and the entire molecule of haloperidol through a classical mechanics energy minimization approach. The third procedure of optimization was carried out using the QM/MM scheme in the ONIOM picture for docking improvement,[65] in such a way that the haloperidol was set as part of the QM layer, while the totality of the D3R residues was set into the MM layer. The resulting structure is referred as quantum mechanics docking input (QMDI) from now on. During the optimization, all hydrogen atoms of the complex, the haloperidol molecule inside the D3R binding pocket with amino acid residues up to a radius of 10 Å from the haloperidol centroid, were allowed to relax. Figure 2 shows the

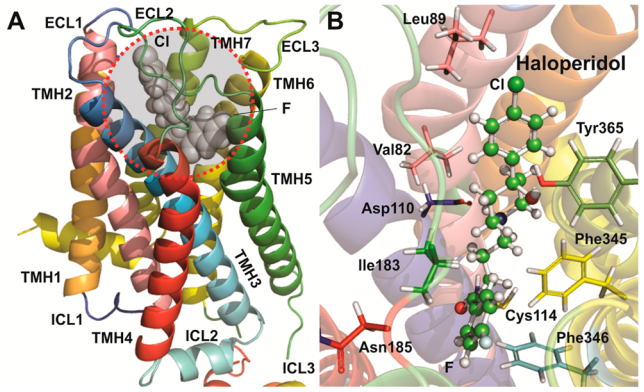

Figure 2. QM/MM optimization after haloperidol docking in D3R. (A) Haloperidol ligand at the binding pocket of D3R, with its atoms depicted as spheres scaled according with the respective van der Waals (VDW) radii. The binding region is enclosed by the dashed red circle. (B) Orientation and structure of haloperidol in its D3R binding pocket. The amino acid residue Asp110 in helix III, which is pivotal to the D3R haloperidol binding, is indicated together with other important residues.

haloperidol at the D3R binding pocket after QMDI optimization. As a matter of fact, the QMDI structure showed significant differences in regard to the conformation of the haloperidol in the binding pocket as compared with the original crude docking result (see Figure 3). The total electronic interaction energy of the system followed the sequence ($E_{QMDI} < E_{CLDI} < E_{CRDI}$), showing that QMDI converged complex is more stable than the CLDI and CRDI ones. Results indicating the dependence of the total binding energy on the binding site radius (measured from the haloperidol centroid) are shown in Figure 4. After the QM/MM optimization, the calculated total binding energy including all residues inside the 10 Å binding radius was −269.5 (−170.1) kcal/mol at the LDA-OBS (GGA-TS) level. For the largest radius, one obtains the total electronic interaction energy, E^T. For r < 4.0 Å, $E(r)$ decreases (the binding increases) strongly, the main contribution coming from the Asp110-ii (N14)H interaction at 4.0 Å (see Figures 4−6). In the 4.0 Å < r < 6.0 Å range, $E(r)$ decreases more weakly, evolving toward a constant value; the main contribution are the His349-iv (C22)H and Tyr365-ii (O9)H at 5.0 Å. For r > 6 Å, while $E(r)$ decreases continuously and oscillates in the LDA case, it oscillates around a mean constant value in the GGA case. The differences obtained when using LDA or GGA is due to the nature of each functional. While within the DFT-LDA approach the long-range interactions are over valuated during the exchange-correlation description, the use of the DFT-GGA-TS functional[80] allows the description of the Van der Walls and hydrogen bonds through an improved description of long-range

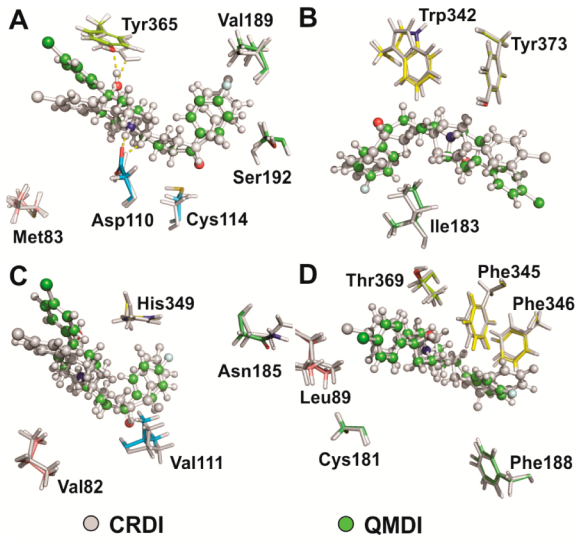

Figure 3. Different superposed views of the D3R-haloperidol geometry before (CRDI) and after (QMDI) QM/MM optimization. (A) Hydrogen bonds of haloperidol with Asp110 and Tyr365 are almost unaffected by QM/MM optimization. (B) Rearrangement of haloperidol and the side chain Ile183 is depicted. (C) Large displacement of haloperidol region I (4-clorophenyl fragment). (D) QM/MM optimization promotes a decrease of the mean distance from haloperidol atoms to Leu89 and Cys181, increasing their attractive interaction with haloperidol.

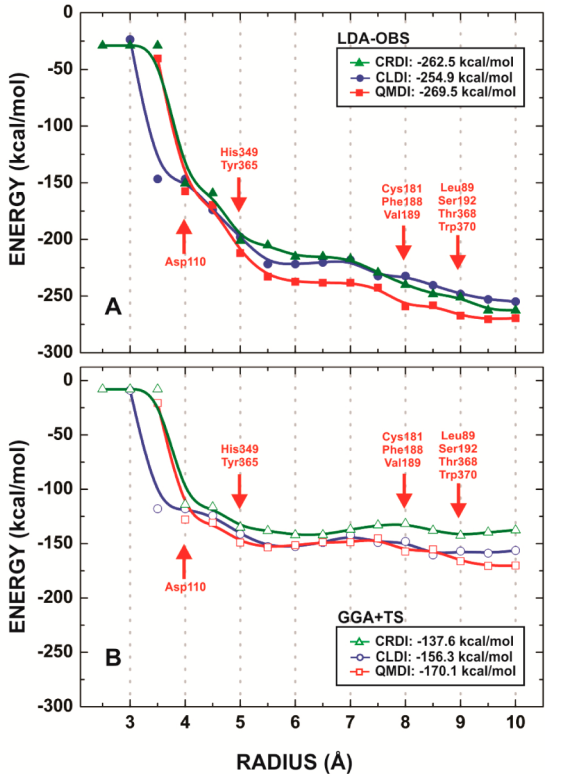

Figure 4. Behavior of the haloperidol−D3R total interaction energy as a function of the binding pocket radius. Computations were performed within the DFT formalism using the (A) LDA-OBS and (B) the GGA-TS functional.

interactions, resulting in a $E(r)$ stabilization for $r > 6$ Å. Besides, the oscillations are due to the DFT difficulty to describe long-range Coulomb interactions related do distant charged residues. Note that for 6.0 Å < r < 10.0 Å, the most relevant interacting residues are Cys181, Phe188, Val189, Leu89, Ser192, Thr368, and Trp370.

The analysis of the final structures generated from the CRDI, CLDI, and QMDI approaches shows the displacement of haloperidol atoms from the original docking pose toward a more stable conformation. For a detailed general perception of this structural rearrangement, one can inspect in the Table S2 of the Supporting Information the interatomic distances of the D3R amino acid residues in the binding pocket to the haloperidol centroid after each optimization strategy. Atomic charges and bond lengths of haloperidol in vacuum, after docking and after classical and QM/MM optimizations were also calculated (Tables S2 and S3, Supporting Information). The charge partitioning methodology known as Hirshfeld population analysis (HPA)[66,81] was adopted as it minimizes the loss of information related to the formation of chemical bonds between atoms in a molecule,[15,82] and produces improved Fukui function indices[83−85] capable of predicting reactivity trends within a molecule better than traditional Mulliken population analysis,[86] natural bond orbital analysis,[87] and fitted electrostatic potentials.[88] However, Hirshfeld charges tend to be too small,[89,90] as Hirshfeld atoms in general resemble the neutral atoms.[91,92] Such limitation, however, can be amended using the iterative Hirshfeld charge technique,[90] which has been successfully applied to the solid state[93] and the discussion of Fukui functions.[94]

The GGA-TS calculated Hirshfeld charges of the individual atoms of haloperidol for the molecular conformation obtained after in vacuum/docking optimizations are depicted in Table S3, and the bond distances of non-hydrogen atoms are show in Table S4. The results are expressed in units of the fundamental charge e, and were calculated using the HPA scheme available in the DMol3 code.[95] They point to O19 and O9(H) as the most negatively charged atomic species (Hirshfeld charges of −0.209e and −0.190e, respectively). The N14(H) nitrogen atom belonging to the hydroxypiperidinyl group, responsible for a large attractive interaction with Asp110 in the binding pocket, is positively charged (0.080e).

Interaction Energy per Individual Amino Acid Residue. DFT calculations[52,53] were employed to assess the relative contribution of each amino acid residue at the binding pocket to the D3R-haloperidol interaction. As the size of the complete protein structure does prevent the use of quantum calculations for the full system, a fragmentation (divide to conquer) approximation was employed. Commonly, fragmentation techniques take into account only the ligand and a given residue with some sort of capping for the dangling bonds, so that the resulting interaction directly reflects the local electronic structure. To improve the accuracy of the method, especially when residues at large distances are included, shielding effects due to neighbor amino acid residues were considered following a procedure established in previous works we published.[58,59,61] Assessments with and without shielding effects included exhibited smaller interaction energy differences for the residues closest to haloperidol, such as Phe345 (3.5 Å), with interaction energy of −11.10 (−12.30) kcal/mol (not) considering shielding, but significant differences for residues at larger distances, such as Cys114 (7.5 Å), which has an interaction energy with (without) shielding effect of 8.80 (−4.00) kcal/mol using the GGA- TS functional. Thus, in order to improve the accuracy of our study, shielding corrections were included in all simulation runs.

dx.doi.org/10.1021/cn500111e | ACS Chem. Neurosci. 2014, 5, 1041−1054

Table 1. Individual Amino Acid Residue Contributions to the Total Haloperidol−D3R Interaction Energy Calculated at the LDA-OBS and GGA+TS Levels[a]

		CRDI			CLDI			QMDI		
receptor segment	residue	LDA	GGA	r (Å)	LDA	GGA	r (Å)	LDA	GGA	r (Å)
TMH1	Tyr36	−11.00	1.00	10.5	−5.00	−6.00	10.0	2.00	2.40	10.0
TMH2	Val78	−1.00	−2.00	9.5	−2.00	0.00	9.5	−1.00	0.00	9.5
	Val82	5.00	10.00	7.5	4.00	8.00	7.5	2.00	3.00	7.5
	Met83	5.00	5.00	10.5	2.00	5.00	10.0	6.00	5.00	6.5
	Val86	−6.80	4.00	8.0	0.80	0.10	7.5	−0.90	2.90	6.5
	Leu89	−4.90	0.80	9.5	−0.70	6.00	9.0	−8.00	−7.00	9.0
TMH3	Phe106	−7.00	−1.00	7.5	−2.00	−2.00	7.0	−2.00	−1.00	6.0
	Val107	−4.00	−3.00	5.5	−5.00	−5.00	5.5	−1.00	−3.00	5.5
	Thr108	−1.00	−1.00	9.0	0.00	1.00	9.0	1.00	1.00	9.0
	Leu109	−1.00	−1.00	9.0	−1.00	−1.00	9.0	−1.20	−1.30	9.5
	Asp110	−112.10	−100.90	4.0	−123.10	−109.00	3.5	−117.20	−107.00	4.0
	Val111	−8.90	1.10	5.0	−7.80	−1.00	5.5	−8.90	5.10	5.5
	Met112	2.00	1.00	9.0	1.00	1.00	9.0	1.00	0.00	9.0
	Met113	2.00	2.00	9.5	2.00	2.00	10.0	1.00	1.00	10.0
	Cys114	8.20	9.00	7.0	4.30	9.00	7.0	5.80	8.80	7.5
	Thr115	1.00	1.00	9.5	0.00	1.00	10.0	1.00	1.00	10.0
TMH4	Leu168	4.00	3.00	7.5	0.00	1.00	8.0	−2.00	1.00	8.0
ECL2	Asn173	0.00	1.00	10.5	0.00	−1.00	10.0	0.00	−2.00	10.0
	Cys181	−3.20	−3.70	9.0	−5.20	−6.70	8.5	−6.60	−6.10	8.0
	Ser182	4.00	5.90	7.0	1.40	3.70	6.5	−2.50	2.90	6.0
	Ile183	−9.50	−5.20	4.0	−8.40	−5.10	4.5	−15.80	−9.70	3.5
	Ser184	1.00	1.00	9.0	0.00	1.00	9.0	1.00	0.00	9.0
	Asn185	−5.00	−4.00	10.0	−1.00	−3.00	10.5	−5.00	−3.00	10.0
TMH5	Phe188	−4.00	−4.70	8.0	−2.00	−3.70	8.5	−2.00	−3.00	8.0
	Val189	−10.00	−6.00	7.5	−8.00	−6.00	7.5	−6.00	−4.00	8.0
	Ser192	−7.30	−4.20	8.5	−7.00	−4.50	9.0	−6.10	−4.90	9.0
	Ser193	−5.50	1.10	9.5	−2.70	0.20	10.0	−1.20	−1.00	10.5
	Ser196	−0.60	−0.90	9.0	−1.70	−0.90	9.5	0.00	0.00	10.0
TMH6	Trp342	−8.90	−4.00	5.0	−10.00	−6.00	5.0	−10.00	−1.00	5.0
	Phe345	−29.00	−8.00	2.5	−23.60	−8.90	3.0	−24.60	−11.10	3.5
	Phe346	−14.30	−9.80	7.0	−11.00	−9.00	7.5	−12.10	−8.30	7.5
	Thr348	−1.00	1.00	9.5	−1.00	0.00	10.0	1.00	1.00	9.5
	His349	−8.50	−2.30	4.5	−5.50	−0.30	4.5	−4.50	−1.30	5.0
	Val350	−3.00	−1.00	9.5	0.00	−2.00	10.0	0.00	−1.00	9.5
	Asn352	2.00	2.00	10.0	2.70	3.30	10.0	2.00	1.00	10.0
	Thr353	0.00	0.00	9.5	0.00	2.00	9.5	1.00	0.00	9.0
TMH7	Tyr365	−11.00	−13.00	5.0	−14.00	−11.00	5.0	−28.00	−16.00	5.0
	Ser366	−2.00	1.00	10.0	−2.00	−3.00	9.5	−2.00	−3.00	9.5
	Thr368	−1.00	−2.00	8.5	−1.00	−3.00	8.5	−1.00	−2.00	9.0
	Thr369	−13.20	−2.80	5.0	−13.30	−0.90	4.5	−12.00	−2.90	4.5
	Trp370	1.00	0.00	9.5	1.00	0.00	9.5	2.00	2.00	9.0
	Gly372	0.00	2.00	8.0	0.00	1.00	8.5	1.00	2.00	8.5
	Tyr373	−10.00	−4.00	6.0	−11.10	−5.60	5.5	−10.90	−6.60	5.5

[a]Energies are given in kcal/mol and the radial distance of each residue do the haloperidol centroid in Å.

The interaction energies of haloperidol with 43 amino acid residues of the D3R binding pocket were calculated, with the results being presented in Table 1. The sum of the individual contribution of residues from the QM/MM optimized structure indicate that the interaction energy does not vary much when the residues located more than 6.0 Å distant from the haloperidol centroid are accounted for. We have closely investigated the interaction of haloperidol with the Cys114 residue, which is located close to Asp110 (Figure 2B), in TMH III, and is part of an important domain for ligand interactions in the D3R binding pocket.[17] The Cys114 amino acid residue is involved in the binding of ligands with, at least, one N-propyl

dx.doi.org/10.1021/cn500111e | ACS Chem. Neurosci. 2014, 5, 1041−1054

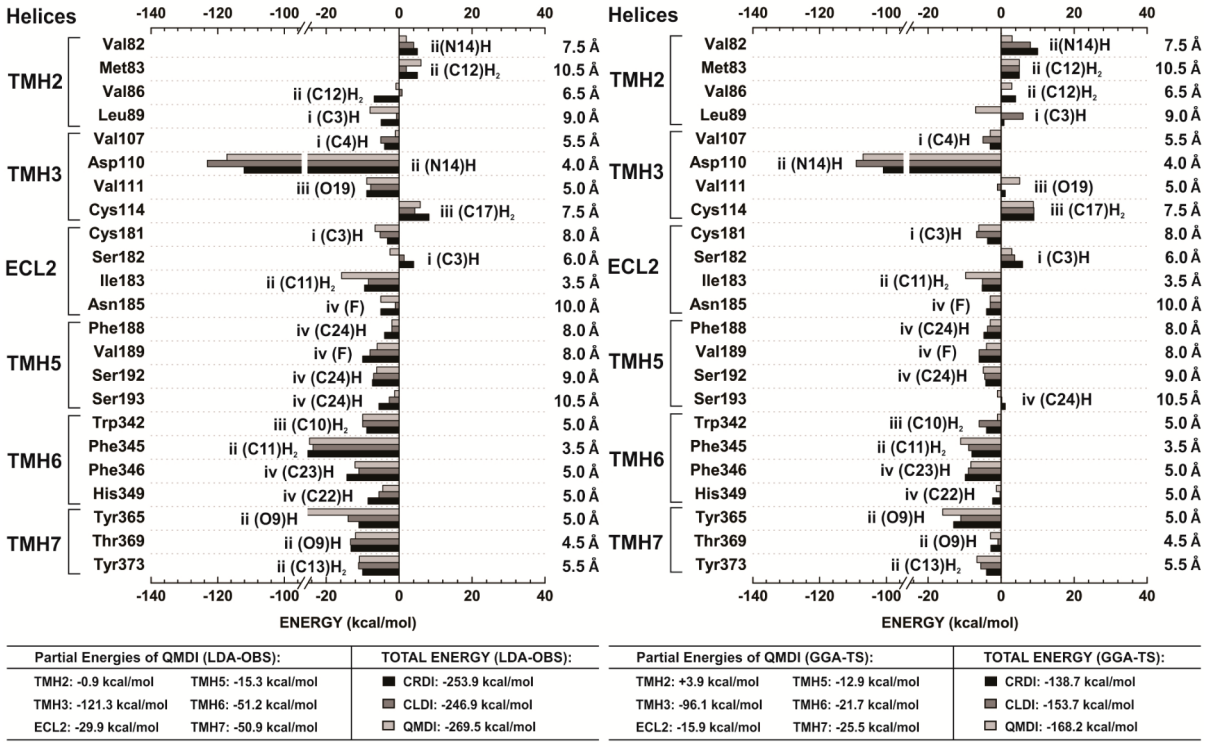

Figure 5. (Left) BIRD panel showing the interaction energy for each amino acid residue in the D3R binding pocket evaluated considering the LDA exchange-correlation functional with OBS dispersion correction. (Right) BIRD panel showing the interaction energy for each amino acid residue in the D3R binding pocket evaluated considering the GGA exchange-correlation functional with TS dispersion correction.

group in its structure. When compared with the wild type, in a competition binding experiment with [^{3}H]-spiperone, the mutated Cys114S receptor showed 272- and 102-fold increases in the *ki* value for two aminotetralin antagonists, UH-232 and AJ-76, respectively.[96] On the other hand, our results show a repulsive interaction of Cys114 (8.80 kcal/mol) with haloperidol obtained within the GGA-TS approach.[72,73]

There are 23 residues with relevant contributions to the binding, the sum of their individual interaction energies being very close to the value of the total binding energy. We were able to identify attractive and repulsive amino acid residues, as one can see from the BIRD panels shown in Figure 5, the former obtained through the LDA exchange-correlation functional with OBS dispersion correction, and the latter through the GGA exchange-correlation functional with TS dispersion correction (see Methods for details of the BIRD panel representation).

It was argued that typical antipsychotics induce a smaller displacement in the transmembrane helix TMH5 of the dopamine D2 receptor in comparison with the other TMHs, while haloperidol nonbonded interactions were larger with helix 3, followed by interactions with helices 6, 7, 2, and 5.[75] In our crude docking simulations, a similar ranking of interactions was obtained: TMH3 > TMH6 > TMH7 > TMH5 > ECL2 ≫ TMH2. In contrast, after the QM/MM geometry optimization, this ranking changed to TMH3 > TMH7 > TMH6 > ECL2 > TMH5 ≫ TMH2. This result suggests that in D3R haloperidol has stronger interaction with helix 5 (GGA-TS calculated interaction energy of −12.90 kcal/mol) than with helix 2 (GGA-TS calculated interaction energy of 3.90 kcal/mol), but weaker interactions with helices 7, 6 and ECL2, which is agreement with the smaller displacement in helix 5 observed for typical antipsychotics. These results also show that haloperidol interacts more strongly with helix 3 where Asp110 is located. This residue is commonly acknowledged as responsible for a strong interaction with the tertiary amine of the ligand.[58,97−101] The value of the Asp110 interaction energy is −117.00 (−107.00) kcal/mol at the LDA-OBS (GGA-TS) level, slightly smaller than that observed in our previous work for eticlopride (−112.21 kcal/mol using GGA-TS).[58] Among the residues in helix 7, Tyr373 and Tyr365 have interaction energies of −10.90 (−6.60) and −28.00 (−16.00) kcal/mol according with the LDA-OBS (GGA-TS) calculations, respectively.

In previous studies, it was suggested that the axial orientation of the haloperidol's hydroxyl group is not essential for binding, but important to the enhancement of the binding at D2R.[102] Our results point that such orientation is also important during the interaction with D3R, responding for the formation of a hydrogen bond with the residue Tyr365 and stabilizing the binding in this region of the binding site. The hydrogen bond between Tyr365 and the alcohol functional group ii(O9)H in haloperidol can be observed before the QM/MM geometry optimization, and after that its length decreases from 2.240 to1.748 Å, which is in agreement with the increase of the interaction energy from −13.00 kcal/mol to −16.00 kcal/mol at the GGA-TS level.

Distances of important D3R residues in the binding pocket to haloperidol after the QM/MM optimization are shown in Figure 6, with it being observed that (i) in helix 6, Phe345 has a $\pi-$cation interaction with region ii (N14) with energy of −24.60 (−11.10) kcal/mol at the LDA-OBS (GGA-TS) approximation; (ii) in region iv (C22)H, Phe346 has an interaction energy of −12.10 (−8.30) kcal/mol and His349 has a $\pi-\sigma$ interaction energy of −4.50 (−1.30) kcal/mol at the LDA-OBS (GGA-TS) level; (iii) the GGA-TS repulsive effect of Ser182 was slighted reduced from 5.90 (CRDI) to 2.90 kcal/

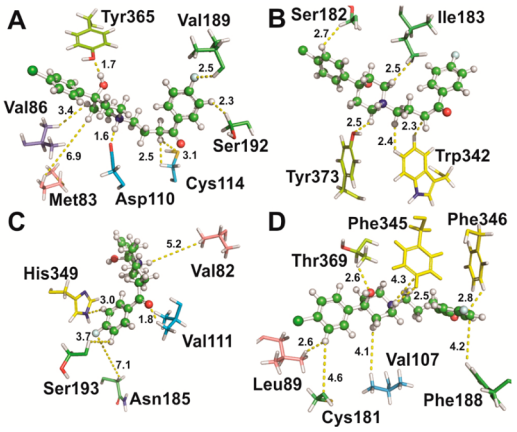

Figure 6. Spatial arrangement of some D3R amino acid residues interacting with haloperidol. Their interaction energies rank among the largest GGA-TS calculated contributions to the total haloperidol−D3R binding energy. Residue−haloperidol distances are depicted by yellow dashed lines.

mol (QMDI), while the LDA-OBS repulsive energy of 4.00 kcal/mol at the CRDI level became an attractive interaction with −2.50 kcal/mol interaction energy in the QMDI picture; (iv) the chlorine atom attached to C2 enhances the QMDI GGA-TS interaction strength with Cys181 (from −3.70 CRDI to −6.10 kcal/mol QMDI) and Tyr365 (from −16.00 to −15.00 kcal/mol); (v) the observed change in the interaction with Leu89 was significant (from 0.80 kcal/mol GGA-TS CRDI to −7.00 kcal/mol GGA-TS QMDI), while the repulsive effect of Ser182 decreased by more than 50% (from 5.90 GGA-TS CRDI to 2.90 kcal/mol GGA-TS QMDI).

These results indicate that, for an improved understanding of the mechanism of interaction of haloperidol with D3R, simple docking calculations are not enough, and further QM/MM optimizations of the drug-binding site system are required.

The extracellular loop 2 is the home of important contributions to the haloperidol−D3R binding, mainly the residues Ile183 and Cys181, both with attractive interaction. Ser182 (Ile183, in D2R), which is close to haloperidol region i(C3)H, in contrast, is repulsive. After the QM/MM geometry optimization, the relative attraction of haloperidol to ECL2 almost doubled as the distance to Ile183 and Cys181 was reduced (Figure 3) in comparison with that within CRDI; interaction with Ser182 may also occur through its interaction with region i of haloperidol.

The residue Ser192 in helix 5, whose replacement by Ala (S192A) decreased the affinity of D3R agonists,[103] has a LDA-OBS (GGA-TS) interaction energy of −6.10 (−4.90) kcal/mol. A similar figure was observed for Val189, with −6.00 (−4.00) kcal/mol of attractive interaction within the LDA-OBS (GGA-TS) picture. Ser193, while showing a repulsive GGA-TS interaction with energy 1.10 kcal/mol in the CRDI picture, changed its interaction state to attractive with GGA-TS interaction energy of −1.00 kcal/mol in the QMDI picture.

When the interaction energies of amino acid residues belonging to the TMH2 region were calculated at the CRDI picture, it was observed a strong repulsive interaction. After QM/MM optimization, however, this repulsive effect was significantly reduced, mainly due to the approximation of haloperidol to the residue Leu89, which showed GGA-TS interaction energy of −7.00 kcal/mol after the QM/MM optimization in comparison with the 0.80 kcal/mol obtained within the CRDI picture. The electron density distribution in the binding cleft of the GGA-TS optimized structure within the QM/MM picture can be observed in Figure 7, where a high (low) electron density is represented in red (blue) color on an electrostatic potential isosurface, with color scales given at the right side.

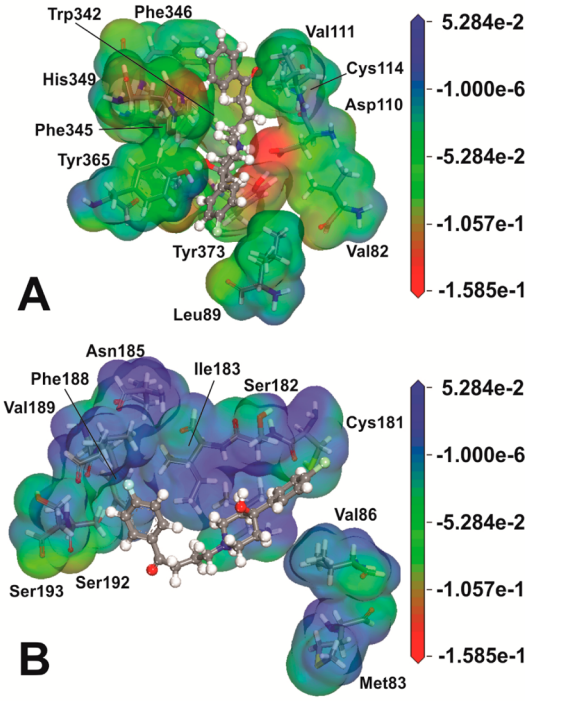

Figure 7. Electrostatic potential isosurfaces of the haloperidol−DR3 binding pocket after the GGA-TS QM/MM optimization. (A) Projected electron densities for the main interacting residues in the D3R binding pocket, highlighting negative charge concentrations at Asp110, Tyr373, and His349. (B) Interacting residues of TMH5 and ECL2 are depicted at the top, while the repulsive residues Met83 and Val86 from TMH2 are also represented right-below. Electrostatic potentials were calculated without taking into account the haloperidol molecule, which was inserted only to visualize which haloperidol regions interact with the residues.

As described in Table S5, 37 out the 43 residues included in our calculations using D3R are conserved in D2R. This similarity in the binding pocket probably accounts for the ability of haloperidol to interact with both receptors, while the six nonconserved residues may be responsible for its greater affinity for D2R. The six D3R nonconserved residues Tyr36, Ser182, Ser184, Val350, Thr353, and Thr368 correspond to residues Leu41, Ile183, Ala185, Ile365, Ile368, and Phe382 in the D2R, respectively. These residues may be involved in the binding through the direct interaction with haloperidol or by promoting changes in the spatial arrangement during the packing of both receptors. In fact, it was observed by Chien et al. that different residues in the extracellular loops give rise to different D2R and D3R electrostatic surfaces in the second binding pocket,[38] which is formed by ECL1/ECL2 and the junction of helices I, II, and VII. Interestingly, it was observed that haloperidol interacts strongly with Tyr373, a conserved residue that forms the second binding pocket (Figure S2). Tyr36 (Leu41 in D2R) is spatially positioned between Tyr373 and Glu95 in D3R and is arranged in the binding pocket closely

dx.doi.org/10.1021/cn500111e | ACS Chem. Neurosci. 2014, 5, 1041−1054

to the 4-clorophenyl fragment, showing a repulsive interaction with haloperidol. Moreover, Tyr36 is located at the extracellular end of TMH1 in a stretch of five nonconserved residues, which should contribute to the differences in the packing between D2R and D3R. Also, the replacement of serines in the ELC2 (Ser182 and Ser184) of D3R, which are amino acids with uncharged side chains, for isoleucine (Ser182-Ile183) and alanine (Ser184-Ala185) in D2R, both with hydrophobic side chains contributing to the explanation of the higher affinity of haloperidol for D2R. In such a scenario, the replacement of Ser182, which is facing the aromatic ring of haloperidol's 4-clorophenyl fragment (region i), by isoleucine would improve the hydrophobic effect in the cavity, increasing the interaction with aromatic ring of the 4-clorophenyl fragment in a similar manner to that observed in the interaction of Ile183 (D3R) and the aromatic ring of the 4-fluorophenyl fragment of haloperidol. The difference between D2R and D3R at the region of the six nonconserved residues (without taking into account spatial arrangement modifications during the packing of helices and loops of D2R) can be observed in Figure S3.

In order to demonstrate the feasibility of designing new haloperidol derivatives using the BIRD panel results as a guideline, we have performed haloperidol modifications in situ (meaning that the haloperidol molecule was modified while docked to the D3R binding site) through the addition of OH or COOH functional groups. Almost all substitutions suggested here for the molecule of haloperidol were investigated in previous studies and their synthesis was described in the literature.[104−109] In order to obtain the derivative with the COOH group at C3, the synthesis may be guided by the route of haloperidol synthesis[105] and the adamantine derivative synthesis (example 52 of patent no WO 00/61569).[104] In this approach, the addition of an amide group at carbon C3 would be followed by hydrolysis with the formation of a carboxylic acid after the condensation of intermediate structures corresponding to regions iii and iv of Figure 1A. These in silico modifications were performed on the structure obtained after the QM/MM optimization procedure (as described above), followed by a classical optimization of haloperidol derivatives and all hydrogen atoms of the D3R receptor.

It is worth to note that the use of the information gathered in this study for the development of derivative/novel compounds through computations performed at the GGA-TS level showed that the insertion of a hydroxyl group (in the equatorial orientation) of C12 of haloperidol (see Figure 1A) enhances the attractive interaction with Asp110 from −107.00 to −121.80 kcal/mol, decreases the repulsive effect of Val86 from 2.90 to 0.50 kcal/mol, and enhances the Met83 repulsion from 5.00 to 8.00 kcal/mol. When a hydroxyl group was added to C24 (in the equatorial orientation), small changes were observed in the haloperidol interaction with Phe188 (from −3.00 to −4.00 kcal/mol) and Ser193 (from −1.00 to −1.50 kcal/mol).

On the other hand, the addition of a hydroxyl group at C3 (in the equatorial orientation) reduced significantly the derivative haloperidol interaction energy with Tyr365, located at the opposite site of the aromatic ring, with reduction of the binding energy from −16.00 to −6.00 kcal/mol. Interaction with Leu89, which is close to C3, was not affected by the hydroxyl substitution, while Cys181 interacted more strongly (interaction energy changing from −6.10 to −10.70 kcal/mol), and Ser182 exhibited a reduction in its repulsive effect (from 2.90 to 0.60 kcal/mol). The COOH group addition at C3 (in the equatorial orientation) reduced the attractive effect of Leu89 (from −7.00 to −3.00 kcal/mol).

As stated above, the use of the per residue interaction's information generated in this study can be a useful guide for the development of derivative and/or novel compounds. Moreover, the methodology here employed can be useful in further experiments for the in silico D3R binding energy evaluation of candidate compounds. Due to the need of consistency, computational cost and to ensure the quality of the results, a comparison of the experimental geometry of D3R with a purely theoretical geometry for D2R was not carried out, as the latter can be significantly different from the real structure. Therefore, this work focused just on the description of haloperidol interactions with D3R, which is the only dopamine receptor with a crystal structure published to the present day. Nevertheless, the approaches described in our work will allow calculating the D2R−ligand interactions when cocrystallized data for this receptor becomes available. The authors highlight that the methodology employed in this study is a powerful tool for theoretical analysis during the prospection of compounds, reducing time and costs in the process. Nevertheless, any results obtained through this approach must be exhaustively tested through in vitro and in vivo assays in order to obtain the pharmacological features and evaluate the clinical effects of the novel/derivative compounds. The authors hope the present work will stimulate efforts to turn our theoretical findings in new improved schizophrenia medicines.

■ CONCLUSIONS

The lack of information on the detailed mechanism surrounding the binding interaction of small molecules in the dopamine receptor D3 motivated us to use computer simulations at the quantum level to investigate the relative energy contribution of individual amino acid residues to the binding of distinct antipsychotic agents. Our aim is to obtain data from typical and atypical agent coupled to D3 in order to map the relevant binding patterns, which will be crucial for the development of new, more potent, and more selective antipsychotic agents. With such perspective, this work is the second of a series of studies to be carried out (ref 58 is the first one), and the next to follow briefly is about the antipsychotic risperidone. Here, by taking advantage of the crystallographic structure of the D3R binding site, we performed docking simulations of haloperidol, a typical antipsychotic agent, followed by the application of a QM/MM energy minimization strategy to improve the quality of the docking result.

The variation of the binding pocket radius r was taken into account to obtain a more accurate estimate of the haloperidol−D3R interaction energy, its value varying from 2.5 to10 Å. Individual interaction energies with haloperidol for each amino acid residue in the binding pocket were thus estimated, showing the pivotal role of Asp110 followed by Tyr365, Phe345, Ile183, Phe346, Tyr373 and Cys114, among others. Conformation analysis pointed out the important role of the axial orientation of the haloperidol's hydroxyl, which has a significant attractive interaction with Tyr365. The haloperidol attractiveness strength to the D3R helices after the GGA-TS QM/MM calculations follows the sequence TMH3 > TMH7 > TMH6 > ECL2 > TMH5 ≫ TMH2, with the interaction with the TMH2 region being a repulsive one. Our results, therefore, are helpful to elucidate, at the molecular level, the binding features of the classical antipsychotic haloperidol with respect to the dopamine D3 receptor, highlighting hot spots to be acted upon

on D3R with the purpose to develop better therapeutic atypical antipsychotics with the ability to blockade this dopamine receptor. Finally, our state of the art simulations indicate that functional substitutions in the 4-clorophenyl and in the 4-hydroxypiperidin-1-yl fragments (such as C3H and C12H hydrogen replacement by OH, OOH, or Cl groups) can lead to haloperidol derivatives with distinct dopamine antagonism profiles. Our results are a first step toward in silico quantum biochemical design and probing of new medications to treat schizophrenia.

METHODS

Structural Data. The calculations performed in this study have taken full advantage of the X-ray crystal structure of human dopamine D3 receptor in complex with eticlopride (PDB ID: 3PBL) at 3.15 Å of resolution.[38] The D3R crystal asymmetric unit cell contains two receptors (A and B) in an antiparallel orientation exhibiting slight shape differences. We arbitrarily chose receptor A to prepare the docking input, replacing the eticlopride molecule by haloperidol in D3R. The preparation of the molecular structure and the protonation state set up at physiological pH of haloperidol were accomplished using the Marvin Sketch code version 5.5.0.1 (Marvin Beans Suite, ChemAxon). To adjust the molecular structure to the protonation state at physiological pH, a single hydrogen atom was added to the amine group of haloperidol, and its charge was adjusted to +1 (electron charge −1). The protonation state of the receptor was adjusted according to results obtained from the PROPKA 3.1 web server tool (http://propka.ki.ku.dk/) and from the Protonation tool in Discovery Studio package.

Molecular Docking. Molecular docking was performed using Autodock4.[63,110,111] To validate the docking protocol adopted in this work, we performed the redocking of eticlopride in the D3 receptor, as described elsewhere.[41,112] Two distinct eticlopride conformations were selected: (i) the ligand in its crystallographic conformation; (ii) the ligand at the minimum energy configuration obtained after classical annealing and quantum DFT geometry optimization. For the docking of haloperidol, the molecule was built up and geometry improved using classical annealing followed by classical and quantum DFT (GGA-TS functional) energy minimization approaches. During the docking of haloperidol, the Lamarckian genetic algorithm (GA) was employed. Docking was performed 20 times using the optimized structure of haloperidol as the input file, a GA with 25 000 000 energy evaluations per run, population size set to 150, and a maximum of 27 000 generations per run. At the end, a thousand poses were obtained (50 poses per output) and clustered using a RMSD tolerance of 1.0 Å^2 using Autodock Tools.[63,113]

Construction of the Haloperidol−D3R Complexes. An isolated haloperidol molecule was first DFT optimized, after which it was docked (as described above) into its D3R binding pocket within a rigid-protein protocol. Among the clusters formed under a RMSD tolerance of 1.0 Å^2, the first pose (of those scored better than the threshold of −10 kcal/mol) were analyzed in order to choose the best representative pose. The haloperidol−D3R complexes were prepared using the dopamine D3 receptor structure after the removal of eticlopride. Every complex was first classically optimized in two consecutive steps: (i) only hydrogen atoms were free to move during optimization; (ii) hydrogen atoms and the haloperidol molecule were free to move during optimization. The classical optimization procedure was performed using the Forcite code with the force field CVFF, the convergence tolerances set to 2.0 × 10^{-5} kcal/mol (total energy variation), 0.001 kcal/mol·Å (maximum force per atom), and 1.0 × 10^{-5} Å (maximum atomic displacement).

Pose Selection. The score of the selected poses was revalidated, in order to ensure the accuracy of the method, through a classical binding energy calculation (E_b) of the best poses from the clusters scored better than the threshold, as described below:

$$E_b = E_{D3R+L} - (E_{D3R} + E_L) \quad (1)$$

At the right side of eq 1, the first term E_{D3R+L} is the total energy of the system formed by haloperidol binding in the D3R; E_{D3R} is the total energy of the D3 receptor alone, while the third term E_L is the total energy of the haloperidol molecule alone.

ONIOM (QM/MM) Optimization. The preparation of the inputs was performed through the TAO package.[114] QM/MM optimization was performed within the two-layer ONIOM framework[115] available in the Gaussian code,[116] employing the hybrid meta exchange-correlation functional M06-2X[117,118] and the 6-311G(d,p) basis set to expand the electronic orbitals for the QM layer. The AMBER force field was used to carry out the MM calculations within an electronic embedding scheme. Ligand charges were assigned using the AMBER force field, and all amino acid residues inside a 10.0 Å radius from the haloperidol centroid were allowed to move freely during the geometry optimization. Haloperidol was considered as belonging to the QM layer, while the entire D3 receptor was treated as belonging to the MM layer.

Classical and DFT Calculations. Hydrogen atoms were inserted into the D3R X-ray structure to fill any dangling bonds, and their positions were optimized classically keeping the other atoms frozen. The classical optimization procedure was performed using the Forcite code with convergence tolerances set to 2.0 × 10^{-5} kcal/mol (total energy variation), 0.001 kcal/mol.Å (maximum force per atom) and 1.0 × 10^{-5} Å (maximum atomic displacement).

Calculations at the DFT level were carried out using the DMol3 code[95,119] to find out the interaction energies of haloperidol with the amino acid residues of D3R inside the binding pocket. The following exchange correlation functionals were employed: (i) local density approximation (LDA-OBS) with PWC parametrization[70] and the OBS dispersion correction scheme,[71] and (ii) the generalized gradient approximation (GGA-TS) with PBE parametrization[72] and TS dispersion correction.[73] A double numerical plus polarization (DNP) basis set was chosen to expand the Kohn−Sham orbitals for all electrons. The orbital cutoff was adjusted to ensure a good balance between accuracy and computational time. The self-consistent field (SCF) convergence threshold was set to 10^{-6} Ha, which is more than enough to reach a well converged electronic structure.

Molecular Fractionation with Conjugate Caps (MFCC) and Shielding Effects. The MFCC scheme is a very useful approach to be achieved an accurate description of biological systems through quantum calculations[43,54−57] without a very high computational cost. In order to avoid missing important interactions, all amino acid residues within an increasing radius from the centroid of haloperidol were taken into account until total energy convergence has occurred. For each amino acid residue, individual sets of capping fragments were formed, including disulfide concaps when necessary. The haloperidol molecule M and the ith amino acid residue R_i interact, with R_i being capped by C_{i-1} and C_{i+1}, the first being the residue covalently bound to the R_i amine group, and the second being the residue covalently bound to the R_i carboxyl group. Hydrogen atoms were added to passivate all dangling bonds.

The electrostatic shielding effect due to the presence of neighbor residues R_b placed between haloperidol and R_i may contribute significantly to affect the M−R_i interaction (see Figure S4 in the Supporting Information). In such a situation, the interaction (binding) energy $E_I[M-R_i]$ is calculated at the DFT level[95,119] in three steps. First, the energy taking into account both the R_b and R_i contributions (Figure S5), $E_I[M-R_bR_i]$ is evaluated according to

$$E_I[M-R_bR_i] = E[M+C_{b-1}R_bC_{b+1} + C_{i-1}R_iC_{i+1}] - E[C_{b-1}R_bC_{b+1} + C_{i-1}R_iC_{i+1}] - E[M+C_{b-1}C_{b+1} + C_{i-1}C_{i+1}] + E[C_{b-1}C_{b+1} + C_{i-1}C_{i+1}] \quad (2)$$

At the right side of eq 2, the first term $E[M+C_{b-1}R_bC_{b+1}+C_{i-1}R_iC_{i+1}]$ is the total energy of the system formed by haloperidol, shielding residues and the residue of interest with caps; $E[C_{b-1}R_bC_{b+1}+C_{i-1}R_iC_{i+1}]$ gives the total energy of the capped residues alone, while the third term $E[M+C_{b-1}C_{b+1}+C_{i-1}C_{i+1}]$ is the total energy of the system formed by the set of caps only and M; finally,

$E[C_{b-1}C_{b+1}+C_{i-1}C_{i+1}]$ is the total energy of the system formed by the isolated caps.

After obtaining $E_I[M-R_bR_i]$, we calculate the interaction energy $E_I[M-R_b]$ between M and the shielding residues R_b (Figure S6) according to

$$E_I[M-R_b] = E[M+C_{b-1}R_bC_{b+1}] - E[C_{b-1}R_bC_{b+1}] - E[M+C_{b-1}C_{b+1}] + E[C_{b-1}C_{b+1}] \quad (3)$$

Here, each term in the second member is obtained from eq 2 by simply removing each occurrence of R_i, $C_{i-1}R_iC_{i+1}$, and $C_{i-1}C_{i+1}$. At last, the corresponding interaction energy $E_I[M\text{-}R_i]$ of M with R_i is calculated as follows:

$$E_I[M-R_i] = E_I[M-R_bR_i] - E_I[M-R_b] \quad (4)$$

Energy Stabilization versus Residue Distance to the Centroid. To avoid using an arbitrary binding pocket size which could risk missing residues with important contributions to the binding energy (this always occurs in general), the binding pocket radius was varied until the total binding energy change was sufficiently small. The total binding energy as a function of the binding site radius was obtained for a 2.5−10 Å radius range with increasing steps of 0.5 Å. Only residues with at least one atom inside an imaginary sphere centered at the drug centroid were taken into account to compute the total binding energy at a chosen radius.

The BIRD Panel. Interaction energies of D3R individual amino acid residues with haloperidol within a given set of approximations were plotted in a panel labeled BIRD (acronym for Binding site, Interaction energy, and Residues Domain) depicting the following: (i) The binding energy (in kcal/mol) of the drug to each amino acid residue at the binding site employing horizontal bars; in this way, one can assess visually the relevance of each residue and the nature of its interaction with the ligand, whether attractive or repulsive; (ii) the most important residues contributing to the binding interaction, which are shown in a column of residues at the left panel side; (iii) the corresponding region of the ligand, i, ii, iii, iv, and so forth which is closer to each residue; and (iv) the distance of each residue to the centroid of the ligand molecule, provided at the right side of the panel.

Molecule Drawing and Images Acquisition. Marvin Sketch code version 5.5.0.1-2011, ChemAxon (http://www.chemaxon.com), was used to draw the 2D haloperidol structure and to predict its protonation state at physiological pH. The images of the resulting poses were obtained using PyMOL 1.3.[120]

■ ASSOCIATED CONTENT

Ⓢ Supporting Information

Redocking of eticlopride in the binding pocket of D3R using the crystallographic and in vacuum optimized ligand conformations. Clusters form docking results under the threshold of −10 kcal/mol and rescoring through classical calculations. Interaction between haloperidol and residues in the secondary binding pocket. Sequence alignment of D3R/D2R binding pocket residues. Spatial comparison between nonconserved residues at D2R−D3R binding pockets. Detailed description of MFCC approach. Haloperidol−D3R residues distance after refinement approaches. Atomic Hirshfeld charges and bond lengths (in Å) of haloperidol non-hydrogen atoms. This material is available free of charge via the Internet at http://pubs.acs.org/.

■ AUTHOR INFORMATION

Corresponding Author

*E-mail: geancarlo.zanatta@gmail.com. Phone: +55 51 3308-3570/3308-5551. Mailing address: Departamento de Bioquímica, Rua Ramiro Barcelos, 2600−anexo, Bairro Santa Cecília, 90035-000−Porto Alegre−RS.

Author Contributions

The manuscript was written through contributions of all authors. All authors have given approval to the final version of the manuscript.

Funding

A.M., E.W.S.C., V.N.F., and C.G. are senior researchers from the Brazilian National Research Council (CNPq), and acknowledge the financial support received during the development of this work from the Brazilian Research Agency CNPq-INCT-Nano(Bio)Simes, Project 573925/2008-9. E.W.S.C. received financial support from CNPq Project 307843/2013-0. C.G. received financial support from CNPq Project 478916/2010-8.

Notes

The authors declare no competing financial interest.

■ ACKNOWLEDGMENTS

The authors would like to thank the Brazilian System of High Performance Processing (Sistema Nacional de Processamento de Alto Desempenho − SINAPAD), especially CESUP-RS and CENAPAD-UFC.

■ REFERENCES

(1) Messias, E. L., Chen, C. Y., and Eaton, W. W. (2007) Epidemiology of schizophrenia: Review of findings and myths. *Psychiatr. Clin. North Am. 30*, 323−338.

(2) Andreasen, N. C. (1993) Positive and Negative Symptoms of Psychosis - a Citation-Classic Commentary on Negative Symptoms in Schizophrenia - Definition and Reliability by Andreasen,N.C., and on Negative V Positive Schizophrenia - Definition and Validation by Andreasen,N.C., Olsen,S. *Cc/Clin Med.*, 8−8.

(3) Andreasen, N. C. (1982) Negative V Positive Schizophrenia - Definition and Validation. *Arch. Gen. Psychiatry 39*, 789−794.

(4) World Health Organization. (2001) *Nations for Mental Health - Schizophrenia and Public Health*, World Health Organization, Geneva.

(5) Roshni Mangalore, M. K. (2007) Cost of schizophrenia in England. *J. Ment. Health Policy Econ. 10*, 23−41.

(6) McEvoy, J. (2007) The costs of schizophrenia. *J. Clin. Psychiatry 68* (Suppl 14), 4−7.

(7) Stahl, S. M. (2003) Describing an Atypical Antipsychotic: Receptor Binding and Its Role in Pathophysiology. *J. Clin. Psychiatry 5*, 9−13.

(8) Strange, P. G. (2001) Antipsychotic Drugs: Importance of Dopamine Receptors for Mechanisms of Therapeutic Actions and Side Effects. *Pharmacol. Rev. 53*, 119−134.

(9) Carlsson, A., and Lindqvist, M. (1963) Effect of Chlorpromazine or Haloperidol on Formation of 3methoxytyramine and Normetanephrine in Mouse Brain. *Acta Pharmacol. Toxicol. 20*, 140−144.

(10) Kapur, S., and Seeman, P. (2001) Does Fast Dissociation From the Dopamine D2 Receptor Explain the Action of Atypical Antipsychotics?: A New Hypothesis. *Am. J. Psychiatry 158*, 360−369.

(11) Chien, W. T., and Yip, A. L. (2013) Current approaches to treatments for schizophrenia spectrum disorders, part I: an overview and medical treatments. *Neuropsychiatr Dis. Treat. 9*, 1311−1332.

(12) Kebabian, J. W., and Calne, D. B. (1979) Multiple receptors for dopamine. *Nature 277*, 93−96.

(13) Jaber, M., Robinson, S. W., Missale, C., and Caron, M. G. (1997) Dopamine receptors and brain function. *Neuropharmacology 35*, 1503−1519.

(14) Rasmussen, S. G., Choi, H. J., Rosenbaum, D. M., Kobilka, T. S., Thian, F. S., Edwards, P. C., Burghammer, M., Ratnala, V. R., Sanishvili, R., Fischetti, R. F., Schertler, G. F., Weis, W. I., and Kobilka, B. K. (2007) Crystal structure of the human beta2 adrenergic G-protein-coupled receptor. *Nature 450*, 383−387.

(15) Ayers, P. W., Morrison, R. C., and Roy, R. K. (2002) Variational principles for describing chemical reactions: Condensed reactivity indices. *J. Chem. Phys. 116*, 8731−8744.
(16) De Lean, A., Stadel, J. M., and Lefkowitz, R. J. (1980) A ternary complex model explains the agonist-specific binding properties of the adenylate cyclase-coupled beta-adrenergic receptor. *J. Biol. Chem. 255*, 7108−7117.
(17) Ostrowski, J., Kjelsberg, M. A., Caron, M. G., and Lefkowitz, R. J. (1992) Mutagenesis of the beta2-Adrenergic Receptor: How Structure Elucidates Function. *Annu. Rev. Pharmacol. Toxicol. 32*, 167−183.
(18) Sibley, D. R., and Monsma, F. J. (1992) Molecular biology of dopamine receptors. *Trends Pharmacol. Sci. 13*, 61−69.
(19) Missale, C., Nash, S. R., Robinson, S. W., Jaber, M., and Caron, M. G. (1998) Dopamine Receptors: From Structure to Function. *Physiol. Rev. 78*, 189−225.
(20) Shimohama, S., Sawada, H., Kitamura, Y., and Taniguchi, T. (2003) Disease model: Parkinson's disease. *Trends Mol. Med. 9*, 360−365.
(21) Joyce, J. N. (2001) Dopamine D3 receptor as a therapeutic target for antipsychotic and antiparkinsonian drugs. *Pharmacol. Ther. 90*, 231−259.
(22) Prasad, S. S., Kojic, L. Z., Li, P., Mitchell, D. E., Hachisuka, A., Sawada, J., Gu, Q., and Cynader, M. S. (2002) Gene expression patterns during enhanced periods of visual cortex plasticity. *Neuroscience 111*, 35−45.
(23) Joyce, J. N., and Meador-Woodruff, J. H. (1997) Linking the Family of D2 Receptors to Neuronal Circuits in Human Brain: Insights into Schizophrenia. *Neuropsychopharmacology 16*, 375−384.
(24) Seeman, P., Wilson, A., Gmeiner, P., and Kapur, S. (2006) Dopamine D2 and D3 receptors in human putamen, caudate nucleus, and globus pallidus. *Synapse 60*, 205−211.
(25) Sokoloff, P., Giros, B., Martres, M.-P., Bouthenet, M.-L., and Schwartz, J.-C. (1990) Molecular cloning and characterization of a novel dopamine receptor (D3) as a target for neuroleptics. *Nature 347*, 146−151.
(26) Chen, J., Levant, B., and Wang, S. (2012) High-affinity and selective dopamine D3 receptor full agonists. *Bioorg. Med. Chem. Lett. 22*, 5612−5617.
(27) Carlsson, J., Coleman, R. G., Setola, V., Irwin, J. J., Fan, H., Schlessinger, A., Sali, A., Roth, B. L., and Shoichet, B. K. (2011) Ligand discovery from a dopamine D3 receptor homology model and crystal structure. *Nat. Chem. Biol. 7*, 769−778.
(28) Löber, S., Hübner, H., Tschammer, N., and Gmeiner, P. (2011) Recent advances in the search for D3- and D4-selective drugs: probes, models and candidates. *Trends Pharmacol. Sci. 32*, 148−157.
(29) Park, W.-K., Jeong, D., Yun, C.-W., Lee, S., Cho, H., Kim, G.-D., Koh, H. Y., Pae, A. N., Cho, Y. S., Choi, K. I., Jung, J. Y., Jung, S. H., and Kong, J. Y. (2003) Pharmacological actions of a novel and selective dopamine D3 receptor antagonist, KCH-1110. *Pharmacol. Res. 48*, 615−622.
(30) Campiani, G., Butini, S., Fattorusso, C., Catalanotti, B., Gemma, S., Nacci, V., Morelli, E., Cagnotto, A., Mereghetti, I., Mennini, T., Carli, M., Minetti, P., Di Cesare, M. A., Mastroianni, D., Scafetta, N., Galletti, B., Stasi, M. A., Castorina, M., Pacifici, L., Vertechy, M., Serio, S. D., Ghirardi, O., Tinti, O., and Carminati, P. (2003) Pyrrolo[1,3]-benzothiazepine-Based Serotonin and Dopamine Receptor Antagonists. Molecular Modeling, Further Structure−Activity Relationship Studies, and Identification of Novel Atypical Antipsychotic Agents. *J. Med. Chem. 47*, 143−157.
(31) Ji, M., Chen, J., Ding, K., Wu, X., Varady, J., Levant, B., and Wang, S. (2005) Design, synthesis and structure−activity relationship studies of hexahydropyrazinoquinolines as a novel class of potent and selective dopamine receptor 3 (D3) ligands. *Bioorg. Med. Chem. Lett. 15*, 1701−1705.
(32) Janssen, P. A. J., Jageneau, A. M., and Schellekens, K. L. (1960) Chemistry and pharmacology of compounds related to 4-(4-hydroxy-4-phenyl-piperidino)-butyrophenone. *Psychopharmacologia 1*, 389−392.
(33) Mutschler, E., Derendorf, H., Schafer-Korting, M., Elrod, K., and Ester, K. S. (1995) *Drug actions: basic principles and therapeutic aspects*, pp 116−125, Medpharm Scientific Publishers, Stuttgart.
(34) Luedtke, R. R., Mishra, Y., Wang, Q., Griffin, S. A., Bell-Horner, C., Taylor, M., Vangveravong, S., Dillon, G. H., Huang, R.-Q., Reichert, D. E., and Mach, R. H. (2012) Comparison of the Binding and Functional Properties of Two Structurally Different D2 Dopamine Receptor Subtype Selective Compounds. *ACS Chem. Neurosci. 3*, 1050−1062.
(35) Seeman, P. (2001) Antipsychotic drugs, dopamine receptors, and schizophrenia. *Clin. Neurosci. Res. 1*, 53−60.
(36) Malmberg, M., and Mohell, N. (1998) Agonist and inverse agonist activity at the dopamine D3 receptor measured by guanosine 5′-gamma-thio-triphosphate-35S-binding. *J. Pharmacol. Exp. Ther. 285*, 119−126.
(37) Roth, B. L., Sheffler, D. J., and Kroeze, W. K. (2004) Magic shotguns versus magic bullets: selectively non-selective drugs for mood disorders and schizophrenia. *Nat. Rev. Drug Discovery 3*, 353−359.
(38) Chien, E. Y. T., Liu, W., Zhao, Q., Katritch, V., Won Han, G., Hanson, M. A., Shi, L., Newman, A. H., Javitch, J. A., Cherezov, V., and Stevens, R. C. (2010) Structure of the Human Dopamine D3 Receptor in Complex with a D2/D3 Selective Antagonist. *Science 330*, 1091−1095.
(39) Andreassen, O. A., and Jørgensen, H. A. (2000) Neurotoxicity associated with neuroleptic-induced oral dyskinesias in rats: Implications for tardive dyskinesia? *Prog. Neurobiol. 61*, 525−541.
(40) Meltzer, H. Y., Thompson, P. A., Lee, M. A., and Ranjan, R. (1996) Neuropsychologic deficits in schizophrenia: Relation to social function and effect of antipsychotic drug treatment. *Neuropsychopharmacology 14*, 27S−33S.
(41) Mohammad, M. K., Al-masri, I. M., Taha, M. O., Al-Ghussein, M. A. S., AlKhatib, H. S., Najjar, S., and Bustanji, Y. (2008) Olanzapine inhibits glycogen synthase kinase-3β: An investigation by docking simulation and experimental validation. *Eur. J. Pharmacol. 584*, 185−191.
(42) Sharma, A., and Shaw, S. R. (2012) Efficacy of Risperidone in Managing Maladaptive Behaviors for Children With Autistic Spectrum Disorder: A Meta-Analysis. *J. Pediatr. Health Care 26*, 291−299.
(43) Gao, A. M., Zhang, D. W., Zhang, J. Z. H., and Zhang, Y. (2004) An efficient linear scaling method for ab initio calculation of electron density of proteins. *Chem. Phys. Lett. 394*, 293−297.
(44) Feng, Z., Hou, T., and Li, Y. (2012) Selectivity and activation of dopamine D3R from molecular dynamics. *J. Mol. Model. 18*, 5051−5063.
(45) Platania, C. B. M., Salomone, S., Leggio, G. M., Drago, F., and Bucolo, C. (2012) Homology Modeling of Dopamine D_2 and D_3 Receptors: Molecular Dynamics Refinement and Docking Evaluation. *PLoS One 7*, e44316.
(46) Abagyan, R., and Totrov, M. (2001) High-throughput docking for lead generation. *Curr. Opin. Chem. Biol. 5*, 375−382.
(47) Sousa, S. F., Fernandes, P. A., and Ramos, M. J. (2006) Protein−ligand docking: Current status and future challenges. *Proteins: Struct., Funct., Bioinf. 65*, 15−26.
(48) Brooijmans, N., and Kuntz, I. D. (2003) Molecular Recognition and Docking Algorithms. *Annu. Rev. Biophys. Biomol. Struct. 32*, 335−373.
(49) Cho, A. E., Chung, J. Y., Kim, M., and Park, K. (2009) Quantum mechanical scoring for protein docking. *J. Chem. Phys. 131*, 134108.
(50) Raha, K., Peters, M. B., Wang, B., Yu, N., Wollacott, A. M., Westerhoff, L. M., and Merz, K. M., Jr. (2007) The role of quantum mechanics in structure-based drug design. *Drug Discovery Today 12*, 725−731.
(51) Zhou, T., Huang, D., and Caflisch, A. (2010) Quantum Mechanical Methods for Drug Design. *Curr. Top. Med. Chem. 10*, 33−45.
(52) Hohenberg, P., and Kohn, W. (1964) Inhomogeneous Electron Gas. *Phys. Rev. 136*, B864.
(53) Kohn, W., and Sham, L. J. (1965) Self-Consistent Equations Including Exchange and Correlation Effects. *Phys. Rev. 140*, A1133.

(54) Chen, X., Zhang, Y., and Zhang, J. Z. H. (2005) An efficient approach for ab initio energy calculation of biopolymers. *J. Chem. Phys. 122*, 184105.
(55) He, X., and Zhang, J. Z. H. (2005) A new method for direct calculation of total energy of protein. *J. Chem. Phys. 122*, 031103−031104.
(56) Zhang, D. W., and Zhang, J. Z. H. (2003) Molecular fractionation with conjugate caps for full quantum mechanical calculation of protein−molecule interaction energy. *J. Chem. Phys. 119*, 3599−3605.
(57) Gordon, M. S., Fedorov, D. G., Pruitt, S. R., and Slipchenko, L. V. (2011) Fragmentation Methods: A Route to Accurate Calculations on Large Systems. *Chem. Rev. 112*, 632−672.
(58) Zanatta, G., Barroso-Neto, I. L., Bambini-Junior, V., Dutra, M. F., Bezerra, E. M., da Costa, R. F., Caetano, E. W. S., Cavada, B. S., Freire, V. N., and Gottfried, C. (2012) Quantum Biochemistry Description of the Human Dopamine D3 Receptor in Complex with the Selective Antagonist Eticlopride. *Proteomics Bioinf. 5*, 155−162.
(59) Barroso-Neto, I. L., Marques, J. P. C., da Costa, R. F., Caetano, E. W. S., Cavada, B. S., Gottfried, C., and Freire, V. N. (2012) Inactivation of Ovine Cyclooxygenase-1 by Bromoaspirin and Aspirin: A Quantum Chemistry Description. *J. Phys. Chem. B 116*, 3270−3279.
(60) Rodrigues, C. R. F., Oliveira, J. I. N., Fulco, U. L., Albuquerque, E. L., Moura, R. M., Caetano, E. W. S., and Freire, V. N. (2013) Quantum biochemistry study of the T3−785 tropocollagen triple-helical structure. *Chem. Phys. Lett. 559*, 88−93.
(61) da Costa, R. F., Freire, V. N., Bezerra, E. M., Cavada, B. S., Caetano, E. W. S., de Lima Filho, J. L., and Albuquerque, E. L. (2012) Explaining statin inhibition effectiveness of HMG-CoA reductase by quantum biochemistry computations. *Phys. Chem. Chem. Phys. 14*, 1389−1398.
(62) Martins, A. C. V., de Lima-Neto, P., Barroso-Neto, I. L., Cavada, B. S., Freire, V. N., and Caetano, E. W. S. (2013) An ab initio explanation of the activation and antagonism strength of an AMPA-sensitive glutamate receptor. *RSC Adv. 3*, 14988−14992.
(63) Morris, G. M., Huey, R., Lindstrom, W., Sanner, M. F., Belew, R. K., Goodsell, D. S., and Olson, A. J. (2009) AutoDock4 and AutoDockTools4: Automated docking with selective receptor flexibility. *J. Comput. Chem. 30*, 2785−2791.
(64) Burger, S. K., Thompson, D. C., and Ayers, P. W. (2010) Quantum Mechanics/Molecular Mechanics Strategies for Docking Pose Refinement: Distinguishing between Binders and Decoys in Cytochrome *c* Peroxidase. *J. Chem. Inf. Model. 51*, 93−101.
(65) Chung, L. W., Hirao, H., Li, X., and Morokuma, K. (2012) The ONIOM method: its foundation and applications to metalloenzymes and photobiology. *Wiley Interdiscip. Rev.: Comput. Mol. Sci. 2*, 327−350.
(66) Hirshfeld, F. L. (1977) *Theor. Chim. Acta 44*.
(67) Martin, Y., and Muchmore, S. (2012) Frozen out: molecular modeling in the age of cryocrystallography. *J. Comput.-Aided Mol. Des. 26*, 91−92.
(68) Król, M., Chaleil, R. A. G., Tournier, A. L., and Bates, P. A. (2007) Implicit flexibility in protein docking: Cross-docking and local refinement. *Proteins: Struct., Funct., Bioinf. 69*, 750−757.
(69) Teague, S. J. (2003) Implications of protein flexibility for drug discovery. *Nat. Rev. Drug Discovery 2*, 527−541.
(70) Perdew, J. P., and Wang, Y. (1992) Accurate and simple analytic representation of the electron-gas correlation energy. *Phys. Rev. B 45*, 13244−13249.
(71) Ortmann, F., Bechstedt, F., and Schmidt, W. G. (2006) Semiempirical van der Waals correction to the density functional description of solids and molecular structures. *Phys. Rev. B 73*, 205101.
(72) Perdew, J. P., Burke, K., and Ernzerhof, M. (1996) Generalized Gradient Approximation Made Simple. *Phys. Rev. Lett. 77*, 3865−3868.
(73) Tkatchenko, A., and Scheffler, M. (2009) Accurate Molecular Van Der Waals Interactions from Ground-State Electron Density and Free-Atom Reference Data. *Phys. Rev. Lett. 102*, 073005.
(74) Chang, Y.-A., Ares, J., Anderson, K., Sabol, B., Wallace, R. A., Farooqui, T., Uretsky, N., and Miller, D. D. (1987) Dopamine agonists: effects of charged and uncharged analogs of dopamine. *J. Med. Chem. 30*, 214−218.
(75) Hjerde, E., Dahl, S. G., and Sylte, I. (2005) Atypical and typical antipsychotic drug interactions with the dopamine D2 receptor. *Eur. J. Med. Chem. 40*, 185−194.
(76) Wang, Q., Mach, R. H., Luedtke, R. R., and Reichert, D. E. (2010) Subtype selectivity of dopamine receptor ligands: insights from structure and ligand-based methods. *J. Chem. Inf. Model. 50*, 1970−1985.
(77) Keller, C., Karr, P., Zandler, M., and Carper, W. R. (1992) Conformational studies of haloperidol. *Struct. Chem. 3*, 195−201.
(78) Reed, L. L., and Schaefer, J. P. (1973) The crystal and molecular structure of haloperidol, a potent psychotropic drug. *Acta Crystallogr., Sect. B 29*, 1886−1890.
(79) Boström, J., Hogner, A., and Schmitt, S. (2006) Do Structurally Similar Ligands Bind in a Similar Fashion? *J. Med. Chem. 49*, 6716−6725.
(80) Reckien, W., Janetzko, F., Peintinger, M. F., and Bredow, T. (2012) Implementation of empirical dispersion corrections to density functional theory for periodic systems. *J. Comput. Chem. 33*, 2023−2031.
(81) Silva, A. M., Silva, B. P., Sales, F. A. M., Freire, V. N., Moreira, E., Fulco, U. L., Albuquerque, E. L., Maia, F. F., Jr., and Caetano, E. W. S. (2012) Optical absorption and DFT calculations in L-aspartic acid anhydrous crystals: Charge carrier effective masses point to semiconducting behavior. *Phys. Rev. B 86*, 195201.
(82) Nalewajski, R. F., and Parr, R. G. (2000) Information theory, atoms in molecules, and molecular similarity. *Proc. Natl. Acad. Sci. U.S.A. 97*, 8879−8882.
(83) Kinkar Roy, R., Hirao, K., Krishnamurty, S., and Pal, S. (2001) Mulliken population analysis based evaluation of condensed Fukui function indices using fractional molecular charge. *J. Chem. Phys. 115*, 2901−2907.
(84) Roy, R. K., Pal, S., and Hirao, K. (1999) On non-negativity of Fukui function indices. *J. Chem. Phys. 110*, 8236−8245.
(85) Parr, R. G., and Yang, W. (1984) Density functional approach to the frontier-electron theory of chemical reactivity. *J. Am. Chem. Soc. 106*, 4049−4050.
(86) Mulliken, R. S. (1955) Electronic Population Analysis on LCAO−MO Molecular Wave Functions. I. *J. Chem. Phys. 23*, 1833−1840.
(87) Foster, J. P., and Weinhold, F. (1980) Natural hybrid orbitals. *J. Am. Chem. Soc. 102*, 7211−7218.
(88) Bonaccorsi, R., Scrocco, E., and Tomasi, J. (1970) Molecular SCF Calculations for the Ground State of Some Three-Membered Ring Molecules: $(CH_2)_3$, $(CH_2)_2NH$, $(CH_2)_2NH^{2+}$, $(CH_2)_2O$, $(CH_2)_2S$, $(CH)_2CH_2$, and N_2CH_2. *J. Chem. Phys. 52*, 5270−5284.
(89) Davidson, E., and Chakravorty, S. (1992) A test of the Hirshfeld definition of atomic charges and moments. *Theoret. Chim. Acta 83*, 319−330.
(90) Bultinck, P., Van Alsenoy, C., Ayers, P. W., and Carbó-Dorca, R. (2007) Critical analysis and extension of the Hirshfeld atoms in molecules. *J. Chem. Phys. 126*, 144111.
(91) Ayers, P. (2006) Information Theory, the Shape Function, and the Hirshfeld Atom. *Theor. Chem. Acc. 115*, 370−378.
(92) Parr, R. G., Ayers, P. W., and Nalewajski, R. F. (2005) What Is an Atom in a Molecule? *J. Phys. Chem. A 109*, 3957−3959.
(93) Verstraelen, T., Sukhomlinov, S. V., Van Speybroeck, V., Waroquier, M., and Smirnov, K. S. (2011) Computation of Charge Distribution and Electrostatic Potential in Silicates with the Use of Chemical Potential Equalization Models. *J. Phys. Chem. C 116*, 490−504.
(94) Bultinck, P., Fias, S., Van Alsenoy, C., Ayers, P. W., and Carbó-Dorca, R. (2007) Critical thoughts on computing atom condensed Fukui functions. *J. Chem. Phys. 127*, 034102.
(95) Delley, B. (2000) From molecules to solids with the DMol3 approach. *J. Chem. Phys. 113*, 7756−7764.
(96) Alberts, G. L., Pregenzer, J. F., and Bin Im, W. (1998) Contributions of cysteine 114 of the human D3 dopamine receptor to

ligand binding and sensitivity to external oxidizing agents. *Br. J. Pharmacol. 125*, 705−710.
(97) Mansour, A., Meng, F., Meador-Woodruff, J. H., Taylor, L. P., Civelli, O., and Akil, H. (1992) Site-directed mutagenesis of the human dopamine D2 receptor. *Mol. Pharmacol. 227*, 205−214.
(98) Soriano-Ursúa, M. A., Ocampo-López, J. O., Ocampo-Mendoza, K., Trujillo-Ferrara, J. G., and Correa-Basurto, J. (2011) Theoretical study of 3-D molecular similarity and ligand binding modes of orthologous human and rat D2 dopamine receptors. *Comput. Biol. Med. 41*, 537−545.
(99) Kalani, M. Y. S., Vaidehi, N., Hall, S. E., Trabanino, R. J., Freddolino, P. L., Kalani, M. A., Floriano, W. B., Kam, V. W. T., and Goddard, W. A. (2004) The predicted 3D structure of the human D2 dopamine receptor and the binding site and binding affinities for agonists and antagonists. *Proc. Natl. Acad. Sci. U.S.A. 101*, 3815−3820.
(100) Javitch, J. A., Fu, D., and Chen, J. (1996) Differentiating dopamine D2 ligands by their sensitivities to modification of the cysteine exposed in the binding-site crevice. *Mol. Pharmacol. 49*, 692−698.
(101) Boeckler, F., and Gmeiner, P. (2006) The structural evolution of dopamine D3 receptor ligands: Structure-activity relationships and selected neuropharmacological aspects. *Pharmacol. Ther. 112*, 281−333.
(102) Sikazwe, D. M. N., Li, S., Mardenborough, L., Cody, V., Roth, B. L., and Ablordeppey, S. Y. (2004) Haloperidol: towards further understanding of the structural contributions of its pharmacophoric elements at D2-like receptors. *Bioorg. Med. Chem. Lett. 14*, 5739−5742.
(103) Kortagere, S., Cheng, S.-Y., Antonio, T., Zhen, J., Reith, M. E. A., and Dutta, A. K. (2011) Interaction of novel hybrid compounds with the D3 dopamine receptor: Site-directed mutagenesis and homology modeling studies. *Biochem. Pharmacol. 81*, 157−163.
(104) Alcaraz, L. F. G. A. R. D. C., Bakewell Road, Loughborough, Leics. LE11 5RH (GB). Furber, Mark[GB/GB]; AstraZeneca R & D Charnwood, Bakewell Road, Loughborough, Leics. LE11 5RH (GB). Mortimore, Michael [GB/GB]; Vertex Pharmaceuticals, 8 Milton Park Abingdon, Oxfordshire OX14 4RY (GB). (19 October 2000) Adamantane Derivatives.
(105) Reynolds, P. J. B., Lee J. (UK). (10 ago. 1982) Synthesis of haloperidol.
(106) Sherman, M. A., Linthicum, D. S., and Bolger, M. B. (1986) Haloperidol binding to monoclonal antibodies: conformational analysis and relationships to D-2 receptor binding. *Mol. Pharmacol. 29*, 589−598.
(107) de Montellano, P. R. O., Kuntz, I. D., Craik, C. S., Furth, P. S., Alvarez, J. C., XCaldera, P. S., DeCamp, D. L., e, L. M. B., De Voss, J., and Salto, R. (1996) Protease-binding compounds and methods of use, Google Patents.
(108) Philip, S. (2007) Enhancement of memory and/or cognition using substituted butyrophenone compounds, Google Patents.
(109) Seeman, P. (2006) Substituted butyrophenone derivatives, Google Patents.
(110) Huey, R., Morris, G. M., Olson, A. J., and Goodsell, D. S. (2007) A semiempirical free energy force field with charge-based desolvation. *J. Comput. Chem. 28*, 1145−1152.
(111) Morris, G. M., Goodsell, D. S., Halliday, R. S., Huey, R., Hart, W. E., Belew, R. K., and Olson, A. J. (1998) Automated docking using a Lamarckian genetic algorithm and an empirical binding free energy function. *J. Comput. Chem. 19*, 1639−1662.
(112) Halperin, I., Ma, B., Wolfson, H., and Nussinov, R. (2002) Principles of docking: An overview of search algorithms and a guide to scoring functions. *Proteins: Struct., Funct., Bioinf. 47*, 409−443.
(113) Sanner, M. F. (1999) Python: A Programming Language for Software Integration and Development. *J. Mol. Graphics Modell. 17* (February), 57−61.
(114) Tao, P., Fisher, J. F., Shi, Q., Vreven, T., Mobashery, S., and Schlegel, H. B. (2009) Matrix Metalloproteinase 2 Inhibition: Combined Quantum Mechanics and Molecular Mechanics Studies of the Inhibition Mechanism of (4-Phenoxyphenylsulfonyl)-methylthiirane and Its Oxirane Analogue. *Biochemistry 48*, 9839−9847.
(115) Vreven, T., Morokuma, K., Farkas, Ö., Schlegel, H. B., and Frisch, M. J. (2003) Geometry optimization with QM/MM, ONIOM, and other combined methods. I. Microiterations and constraints. *J. Comput. Chem. 24*, 760−769.
(116) Frisch, M. J., Trucks, G. W., Schlegel, H. B., Scuseria, G. E., Robb, M. A., Cheeseman, J. R., Scalmani, G., Barone, V., Mennucci, B., Petersson, G. A., Nakatsuji, H., Caricato, M., Li, X., Hratchian, H. P., Izmaylov, A. F., Bloino, J. Z., Zheng, G., Sonnenberg, J. L., Hada, M. E., M;, Toyota, K., Fukuda, R., Hasegawa, J., Ishida, M., Nakajima, T., Honda, Y., Kitao, O., Nakai, H., Vreven, T., Montgomery, J. A., Jr., Peralta, J. E., Ogliaro, F., Bearpark, M., Heyd, J. J., Brothers, E., Kudin, K. N., Staroverov, V. N., Kobayashi, R., Normand, J., Raghavachari, K., Rendell, A., Burant, J. C., Iyengar, S. S., Tomasi, J., Cossi, M., Rega, N., Millam, J. M., Klene, M., Knox, J. E., Cross, J. B., Bakken, V., Adamo, C., Jaramillo, J., Gomperts, R., Stratmann, R. E., Yazyev, O., Austin, A. J., Cammi, R., Pomelli, C., Ochterski, J. W., Martin, R. L., Morokuma, K., Zakrzewski, V. G., Voth, G. A., Salvador, P., Dannenberg, J. J., Dapprich, S., Daniels, A. D., Farkas, Ö., Foresman, J. B., Ortiz, J. V., Cioslowski, J., and Fox, D. J. (2009) *Gaussian 09*, Revision A.1, Gaussian, Inc., Wallingford CT.
(117) Zhao, Y., and Truhlar, D. G. (2008) Exploring the Limit of Accuracy of the Global Hybrid Meta Density Functional for Main-Group Thermochemistry, Kinetics, and Noncovalent Interactions. *J. Chem. Theory Comput. 4*, 1849−1868.
(118) Zhao, Y., and Truhlar, D. (2008) The M06 suite of density functionals for main group thermochemistry, thermochemical kinetics, noncovalent interactions, excited states, and transition elements: two new functionals and systematic testing of four M06-class functionals and 12 other functionals. *Theor. Chem. Acc. 120*, 215−241.
(119) Delley, B. (1990) An all-electron numerical method for solving the local density functional for polyatomic molecules. *J. Chem. Phys. 92*, 508−517.
(120) (2010) *The PyMOL Molecular Graphics System*, Version 1.3r1, Schrödinger, LLC, Cambridge, MA.